CrystEngComm

Liquid exfoliation of five-coordinate layered titanate $K_2Ti_2O_5$ single crystals in water

Journal:	*CrystEngComm*
Manuscript ID	CE-ART-04-2022-000512.R2
Article Type:	Paper
Date Submitted by the Author:	16-Jun-2022
Complete List of Authors:	HAYASHI, Fumitaka; Shinshu University, Faculty of Engineering Furui, Kenta; Shinshu University, Faculty of Engineering Tatewaki, Nanako; Shinshu University, Faculty of Engineering Sudare, Tomohito; Shinshu University, Research Initiative for Supra-Materials (RISM) Kashiwazaki, Maru; Shinshu University, Faculty of Engineering Shiiba, Hiromasa; Shinshu University, Department of Materials Chemistry Tanaka, Hideki; Shinshu University, Research Initiative for Supra-Materials Koyama, Michihisa; Shinshu University Faculty of Engineering Terashima, Chiaki; Tokyo University of Science, Research Institute for Science & Technology Teshima, Katsuya; Shinshu University, Department of Materials Chemistry; Shinshu University, Center for Energy and Environmental Science

ARTICLE

Liquid exfoliation of five-coordinate layered titanate $K_2Ti_2O_5$ single crystals in water

Received 00th January 20xx,
Accepted 00th January 20xx

DOI: 10.1039/x0xx00000x

Fumitaka Hayashi,*[ab] Kenta Furui,[a] Nanako Tatewaki,[a] Tomohito Sudare,[c] Maru Kashiwazaki,[a] Hiromasa Shiiba,[c] Hideki Tanaka,[c] Michihisa Koyama,[c] Chiaki Terashima[c,d] and Katsuya Teshima*[abcd]

Liquid exfoliation is a scalable and effective technique for preparing two-dimensional materials but suffers from several issues, including low yields and lack of control over the lateral size of the nanosheets. Herein, we report the flux-evaporation-assisted growth of millimeter-sized $K_2Ti_2O_5$ (KTO) single crystals and their liquid-phase hydrothermal exfoliation to form nanosheet colloids in water. The parent millimeter-long KTO single crystals were grown from a KCl–KOH flux at 900 °C in air flow, and several solvents for the exfoliation of KTO were investigated. As a result, H_2O was found to be the best solvent for exfoliation. Field-emission scanning electron microscopy analysis of a typical 2D KTO nanosheet revealed that its lateral size was 5–15 μm, consistent with dynamic light scattering results. Scanning probe microscopic analysis showed that there was some dispersion in the degree of exfoliation of the nanosheets and that approximately 60% of the nanosheets had thicknesses of less than 10nm. In addition, X-ray absorption near edge structure (XANES) measurements of the KTO nanosheet colloid provide evidence that the KTO crystals undergo partial hydrolysis in water to generate hydroxyl groups on the surface, which weaken the interactions between the anionic frameworks and interlayer cations and accelerate exfoliation. Density functional theory calculations of the exfoliation energy reveal that this hydrolysis reaction decreased the exfoliation energy compared to that of bare KTO.

Introduction

Two-dimensional (2D) materials have attracted the attention of chemists and physicists because of their unexpected physical, chemical, electronic, and optical properties.[1,2] These nanomaterials have been widely applied in the energy and environmental fields. For instance, 2D materials can be used as electro- and photo-catalysts, battery electrode materials, adsorbents, separation membranes, and transistors.[3] These 2D materials have atomic or molecular-level thicknesses and infinite planar lengths with a lateral length of (sub)micrometers. Various 2D materials have been prepared via the top-down approach from various precursors, including transition metal dichalcogenides, layered double hydroxides, layered transition metalates, and MAX phase compounds.[1] The well-established synthetic methods for 2D materials include micromechanical cleavage, mechanical force-assisted liquid exfoliation, ion intercalation/exchange-assisted liquid exfoliation, selective-etching assisted exfoliation, and wet-chemical synthesis.[2] Among the various methodologies, chemical exfoliation in a solvent is a scalable and powerful tool for the efficient production of 2D materials. However, there remain several challenges; for example, the control over the yield, the lateral size, and crystallinity must be improved.[4] With respect to the production of TiO_2-based 2D materials, several chemical techniques, such as the introduction of protons into interlayers and subsequent acid–base reactions with bulky organic bases such as tetrabutyl ammonium hydroxide (TBAOH) are required to exfoliate the parent layered metalates including titanates because the interlayer electrostatic interactions are strong.[5] In the case of $K_2{}^{[5]}TiO_3$, which has a chain structure of TiO_5 polyhedra (here, "$^{[5]}$" indicates the coordination number (CN) of Ti),[6] its immersion in an aqueous nitric acid solution at pH ≤ 1 leads to the formation of a colloidal suspension of nanosheets. Therefore,

[a] Department of Materials Chemistry, Faculty of Engineering, Shinshu University, 4-17-1 Wakasato, Nagano 380-8553, Japan. E-mail: fhayash@shinshu-u.ac.jp
[b] Global Aqua Innovation Center, Shinshu University, Wakasato, Nagano 380-8553, Japan.
[c] Research Initiative for Supra-Materials (RISM), Shinshu University, 4-17-1 Wakasato, Nagano 380-8553, Japan. E-mail: teshima@shinshu-u.ac.jp
[d] Research Center for Space System Innovation, Tokyo University of Science, 2641 Yamazaki, Noda, 278-8510, Japan

† Electronic Supplementary Information (ESI) available: Immersion test results (Table S1), core-hole positions for XANES simulations (Fig. S1), slab models for exfoliation energy calculations (Fig. S2), XRD patterns (Figs. S3 and S4), AFM image (Fig. S5) dynamic light scattering analysis result (Fig. S6), $K_2Ti_2O_5$-H_2O crystal structure (Fig. S7). This material is available free of charge via the Internet at http://pubs.acs.org. See DOI: 10.1039/x0xx00000x

a fundamental question is whether the layered titanates can be exfoliated in eco-friendly solvents without the use of acids and bulky bases, as is the case for the exfoliation of transition metal dichalcogenides and Ca_2N in common solvents such as N-methylpyrrolidone (NMP), 2-propanol, and 1,3-dioxane.[7,8]

Layered titanates are generally represented as $A_2O \cdot nTiO_2$, where A is the alkali metal ion and n = 2, 4, 6, or 8.[9] The crystal structures with interlayer gallery space are strongly dependent on the kinds of alkali metal ions and the number *n*. Herein, we focus on the five-coordinate layered titanate $K_2^{[5]}Ti_2O_5$ (KTO) as a starting material.[10] The CN of KTO is five, whereas those of previously reported lepidocrocite-type $H_xTi_{2-x/4}\square_{x/4}O_4 \cdot H_2O$ (□: vacancy; x = 0.7)[11] and $Na_2Ti_3O_7$[12] are both six. Generally, the exfoliation mechanism is assumed to occur via the intercalation of solvent molecules with the five-coordinate Ti species, thus weakening the electrostatic interactions between the anionic metalate frameworks and interlayer cations, resulting in the exfoliation of KTO crystals. The resultant 2D materials are mainly composed of TiO_2, which could have photo- and electrochemical properties similar to those of TiO_2 anatase and bronze.[5,13]

Herein, we demonstrate the flux-evaporation-assisted growth of millimeter-sized KTO single crystals and the exfoliation of the resultant KTO crystals without the use of strong acids and bases or mechanical techniques. This is the first example of exfoliation of layered titanate in the absence of strong acids and bases. The exfoliation conditions were examined using various solvents and a hydrothermal autoclave reactor. A possible exfoliation mechanism for KTO is discussed based on spectroscopic characterization and theoretical calculations.

Experimental

All reagents were purchased from Wako Pure Chemical Industries. Reagent-grade TiO_2 was used as the Ti source, and K_2CO_3, KCl, K_2SO_4, and KOH were used as the K sources and fluxes. The molar ratio of KCl to KOH was 3:7 in the mixed flux, and the solute concentration ranged from 20 to 100 mol%. For the flux-cooling method, a homogenous mixture of precursors and flux (approximately 20 cm^3 in volume) was tightly sealed with a lid and heated in air in an electric furnace. A plug-flow furnace was used for the flux evaporation method, for which the air flow rate was 500 mL min^{-1}. A holding temperature of 900 °C was applied for 12 h. The heating and cooling rates were 300 and 200 °C h^{-1}, respectively. For comparison, a $K_2Ti_4O_9$ sample was prepared following a literature method.[14] Note that the flux is not completely evaporated under these flux growth condition.

The exfoliation of the flux-grown KTO crystals was performed by their immersion in various solvents under ambient or hydrothermal conditions for 3 days. Under ambient conditions, KTO crystals (50–100 mg) and solvent (10 mL) were added to the vessel and allowed to stand at room temperature for 3 days. under hydrothermal conditions, the KTO-solvent mixture was sealed in a Teflon-lined vessel and maintained at 120 °C for 3 days. After the treatment, the solution was transferred to a glass beaker and allowed to stand for 5 min, followed by the recovery of the supernatant liquid for the further analysis of the nanosheet colloidal solution.

X-ray diffraction (XRD) patterns were collected using a Smart diffractometer (Rigaku, Japan) with monochromated Cu-K_α radiation (λ = 0.15418 nm, 40 kV, 30 mA). Field-emission scanning electron microscopy (FE-SEM) images and energy dispersive X-ray (EDX) spectrometry data were obtained using a JSM-7600F (JEOL, Japan). Scanning probe microscopy (SPM, SPM-Nanoa, Shimadzu) and atomic force microscopy (AFM, Agilent Technologies, 5500 Scanning Probe Microscope) were used to obtain the thickness profiles of the KTO nanosheets. The Ti *K*-edge X-ray absorption fine structure (XAFS) spectra were acquired in fluorescence (for KTO nanosheets) and transmission (for parent KTO and reference samples) modes at beamline BL5S1 of the Aichi Synchrotron Radiation Center and at beamline BL-12C of the Photon Factory, High Energy Accelerator Research Organization KEK, in Tsukuba. The incident beam energy was selected using a Si(111) monochromator. Energy calibration was performed by simultaneously measuring the spectra of an appropriate metal foil sample. The solution samples were sealed in polyethylene bags. The parent KTO and reference samples were mixed with an appropriate amount of reagent-grade boron nitride (BN, Wako Pure Chemical Industries) and pelletized. Additional spectra of the reference standards were also measured to facilitate the interpretation of the XAFS data. Data analysis was carried out using Athena, part of the Demeter package.[15]

To simulate the X-ray absorption near edge structure (XANES) spectra, density functional theory (DFT) calculations were carried out using the plane-wave pseudopotential method in the Cambridge Serial Total Energy Package (CASTEP).[16] The crystal structures of the KTO and KTO-derivatives were fully optimized using a unit cell of 18 or more atoms (corresponding to Z = 2 formula units). The generalized gradient approximation Perdew–Burke–Ernzerhof functional revised for solids (PBEsol-GGA) was used to model the exchange and correlation energies. The cutoff energy was 800 eV, and the total number of *k*-point for the respective models was >80. For XANES simulation, we employed the on-the-fly generated pseudopotentials to describe the core electrons of K, T, O and H atoms using a cutoff energy of 800 eV. Theoretical XANES spectra were obtained within the electronic-dipole-allowed transitions, where core-hole effects were considered.[17,18] To reduce the interactions between core-holes, XANES spectra were calculated using supercells (> 1 nm^3), for which a (1× 1 × 1) grid was used. The core-hole positions of the KTO and KTO-derivatives are specified in Fig. S1.

The exfoliation energies were calculated by using DFT carried out in the Vienna Ab Initio Simulation Package (VASP)[19,20] with the modified PBEsol-GGA functional[21,22] and the projector-augmented wave (PAW) method.[23] All calculations were performed using a unit cell of 18 or more atoms (corresponding to Z = 2 formula units)

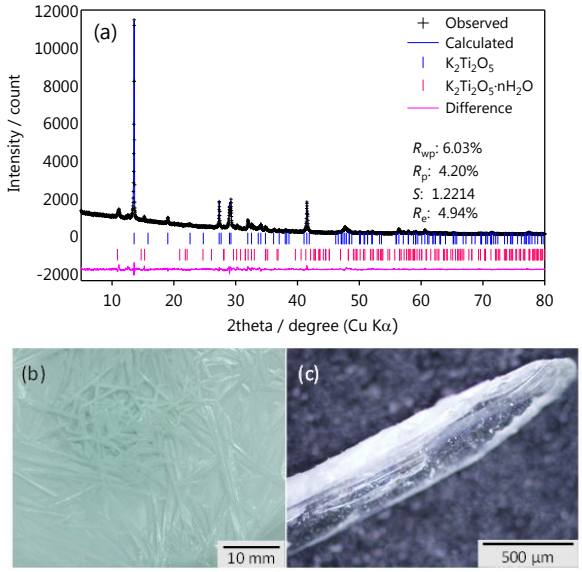

Fig. 1 (a) Observed, calculated, and difference XRD Rietveld profiles for the $K_2Ti_2O_5$ crystals. Condition: Flux = KCl–KOH, heating rate = 300 °C · h^{-1}, holding temp. = 900 °C, holding time = 12 h, [solute] = 50 mol%, and air flow rate = 500 mL · min^{-1}. (b) Optical micrograph and (c) SEM images of single-crystalline $K_2Ti_2O_5$.

based on the monoclinic lattice of KTO. The exfoliated models of these layered compounds were simulated by inserting a vacuum layer along the direction perpendicular to a single layer, as reported previously.[24,25] An infinite planar structure was represented by a periodic slab model with a slab distance of 2 nm to ensure that there were no interactions between the slabs. The slab models of the $K_2Ti_2O_5$ and $K_2Ti_2O_5$ derivatives are summarized in Fig. S2. The exfoliation energy, ΔE_{exf} (also known as the binding energy), was calculated using Eq. 1.

$$\Delta E_{exf} = (E_{slab} - E_{bulk})/2A \quad (1)$$

Here, E_{slab} and E_{bulk} are the total energies of the model structures, and A is the basal area of the exfoliated structures. The cutoff energy was set at 500 eV. The total numbers of k-point for the respective models were >50. The crystal structures were modeled and visualized using VESTA.[26]

Results and Discussion

First, we examined the flux growth of single-phase $K_2Ti_2O_5$ crystals. We examined the flux growth conditions using several types flux (KCl, KCl–KOH, and KCl-K_2SO_4), different holding temperatures, and various degrees of flux evaporation, and we found that the use of the mixed KCl–KOH flux at 900 °C in the flow of air was effective for the growth of submillimeter-sized KTO single crystals. Fig. 1a shows the XRD pattern of KTO crystals grown from KCl–KOH flux at 900 °C as well as the Rietveld refinement results. The XRD pattern of KTO was determined to be consistent with those of $K_2Ti_2O_5$ and $K_2Ti_2O_5 \cdot nH_2O$, indicating the absence of impurity phases. The diffraction profiles of the two main phases were indexed to the monoclinic

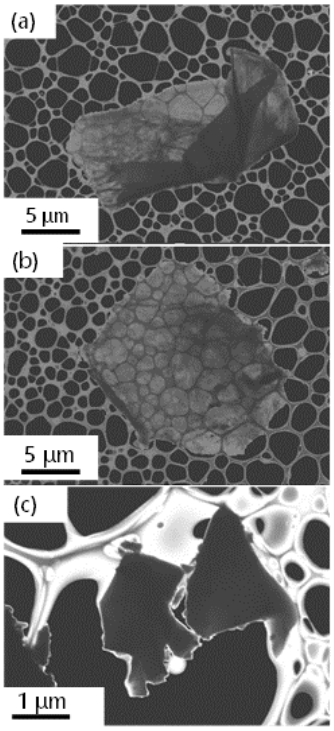

Fig. 2 FE-SEM images of $K_2Ti_2O_5$ samples after immersion in (a) water and (b) acetone, and that of (c) $K_2Ti_4O_9$ crystals after immersion in water. Conditions: solid/solution ratio = 5.0 g · L^{-1}, temperature = 120 °C, and holding time = 3 days.

system as follows: (i) for $K_2Ti_2O_5$, a = 1.13610(17) nm, b = 0.37940(6) nm, and c = 0.661836(15) nm and β = 99.842(4)°, and (ii) for $K_2Ti_2O_5 \cdot nH_2O$, a = 1.2709(11) nm, b = 0.3774(3) nm, and c = 0.8534(7) nm and β =108.30(9)°. Note that KTO crystals readily undergo hydrolysis.[27] For instance, the position of the (001) diffraction peak is shifted to 10.98° from 13.60° after storage for 1 day under ambient conditions, yielding a basal spacing of approximately 0.78 nm, as shown in Fig. S3. The observed values for the main $K_2Ti_2O_5$ phase are comparable with the literature values of a = 1.1374 nm, b = 0.3799 nm, and c = 0.6616 nm and β = 100.10°.[10] The optical micrograph of the KTO crystal in Figs. 1b and 1c shows the formation of needle-like KTO crystals of 10–30 mm in length. Thus, this flux growth technique using flux evaporation is superior to conventional solid-state reaction methods,[28] especially for obtaining large KTO crystals.

Next, we studied the exfoliation of bulk KTO crystals. We initially examined 13 solvents with different functional groups, and polar and non-polar solvents were employed for the exfoliation, as reported previously.[7,8] Initially, we suspended the bulk KTO crystals in each solvent and the resulting colloidal suspension was kept for 3 days under ambient conditions. The Tyndall effect was utilized to screen the solvents for their exfoliation ability, and the results are summarized in Table S1. Non-polar solvents such as chloroform and toluene (entries 1 and 3 in Table S1) and some polar solvents such as ethylene carbonate and tetrahydrofuran (entries 5 and 12) did not result in the appearance of the Tyndall effect. On the other

hand, in the suspensions prepared using water and acetone, a strong Tyndall effect was observed (entries 9 and 13). Highly-polar water and acetone molecules might interact with five-coordinate Ti species in the metalate frameworks, resulting in weakened electrostatic interactions between K^+ and anionic slabs. Therefore, we used water as a dispersion medium because of its environmental friendliness and low cost. We then used an ultrasonic homogenizer sonicator and centrifugal separator with water to examine the effect of the application of mechanical force; however, efficient exfoliation did not occur. Therefore, we explored another approach, that is, the use of a hydrothermal reactor to accelerate the exfoliation reaction. The resulting mixture was not stirred or centrifuged to prevent any reduction in the size of the nanosheets. The concentration of the resulting KTO nanosheets was approximately 8 ppm and the yield of nanosheet was about 0.5%. The yield could be potentially increased by changing the treatment conditions. To confirm the specificity of this reaction for the five-coordinated $K_2^{[5]}Ti_2O_5$ crystal structure, we employed another layered titanate $K_2^{[6]}Ti_4O_9$[13] having $CN_{Ti} = 6$ for comparison.

Figs. 2a and 2b show the FE-SEM images of $K_2Ti_2O_5$ crystals after immersion in pure water and acetone under hydrothermal/solvothermal conditions. The light-gray color of both images indicates the transmission of the electron beam, indicating significant exfoliation. The sheet sizes of both titanate samples were greater than 5 μm in lateral size. The side of the KTO nanosheet in Fig. 2a is scrolled because of its softness and stabilization by minimizing electrostatic repulsion, as observed for nanosheets of hexaniobate.[29] Fig. 2c shows the FE-SEM images of $K_2Ti_4O_9$ crystals after immersion in water under hydrothermal conditions. As shown, the electron beam did not pass through the KTO crystal, indicating that exfoliation had not occurred. The sharp difference between the $K_2Ti_2O_5$ and $K_2Ti_4O_9$ systems indicates the importance of the crystal structure of the host material for exfoliation. The XRD pattern of KTO nanosheet sample after evaporation to dryness is shown in Fig. S4. A very weak and broad diffraction peaks can be seen at approximately 11.20 and 47.84°, and these peaks are consistent with those for $K_2Ti_2O_5 \cdot nH_2O$ in Fig. 1.

To evaluate the thickness of the KTO nanosheet, we carried out AFM and SPM analyses. Fig. 3 shows AFM and SPM images of a titanate nanosheet derived from KTO crystal under hydrothermal conditions. Analysis of cross sections in Fig. 3 showed that the thickness of the titanate sheets was approximately 3-4 nm, which corresponds to 5-7 layers of the $[Ti_2O_5]^{2-}$ sheet (approximately 0.65 nm), as estimated from the known crystal structure. Fig. S5 shows another AFM image and an analysis of the statistical distribution of the KTO nanosheet thickness. As shown, there was some dispersion in the degree of exfoliation in the formed KTO nanosheets. This variation in the thickness might be attributed to the staging exfoliation frequently observed for layered materials. The KTO crystals were not exfoliated to a single layer under the present conditions, but the exfoliation proceeded to a significant degree.

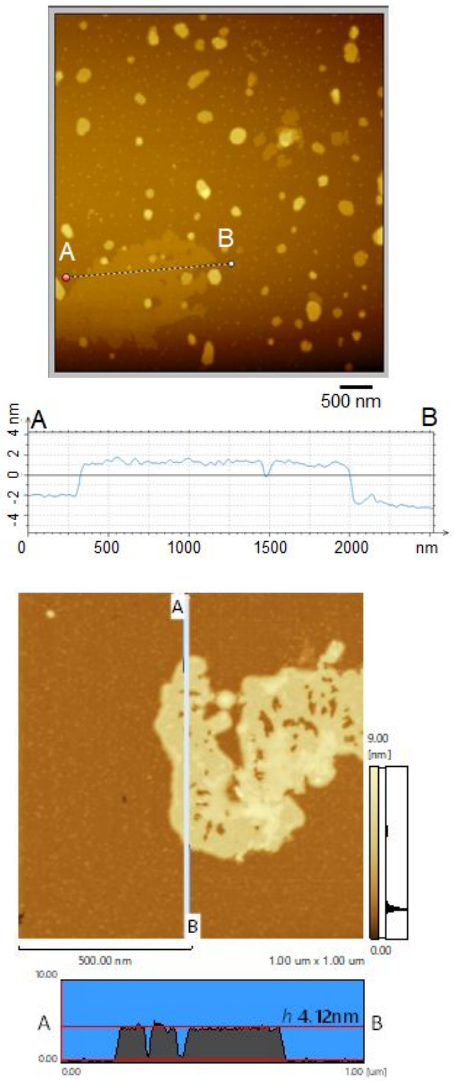

Fig. 3 (Top) AFM and (Bottom) SPM images of the $K_2Ti_2O_5$ sample prepared by dispersing the colloidal nanosheet suspension on a Si surface.

With regard to the shape of nanosheet, the shape became round. We couldn't understand the reason for this change, but one explanation is that the morphology change could be attributed to hydration reaction of KTO with H_2O which could enforce amorphization of KTO crystal.

Fig. S6 shows the particle size distribution of the KTO nanosheets measured by dynamic light scattering (DLS). The results show an almost monomodal distribution centered at approximately 10 μm (Fig. S6). According to Coleman et al.,[30] the hydrodynamic radius, *a*, is correlated with the length (diameter) of the nanosheet when approximating the nanosheets as disks. Based on this empirical relationship, the DLS result is consistent with those shown in Fig. 2a.

We next studied the changes in the local structure of the Ti species in the KTO crystal after exfoliation to understand its effects on the crystal structure. Fig. 4a shows the Ti *K*-edge XANES spectra of the

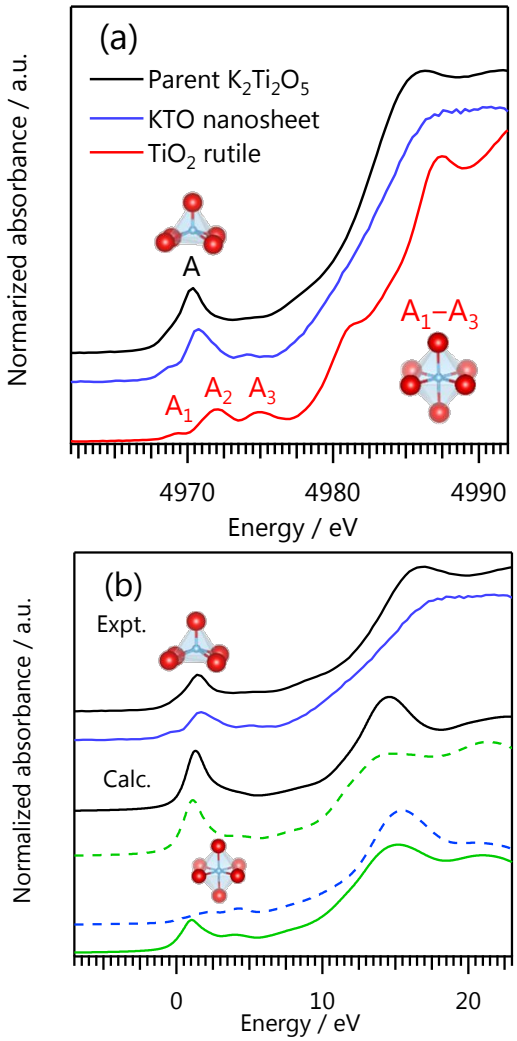

Fig. 4 (a) Experimental pre-edge peaks in the Ti *K*-edge XANES spectra of the starting bulk KTO sample (black), KTO nanosheet colloidal suspension (blue), and TiO_2 rutile (red). The peak labels are according to the literature.[32,34] (b) Experimental and calculated pre-edge peaks in the Ti *K*-edge XANES spectra for $K_2Ti_2O_5$ (black solid line), the KTO nanosheet colloid (blue solid line), model compound $K_2Ti_2O_5$-H_2O (hole position = $^{[5]}$Ti, green dashed line), $K_2Ti_2O_5$-H_2O (hole position = $^{[6]}$Ti, blue dashed line), and $K_2Ti_2O_5$-H_2O (hole positions = $^{[5]}$Ti and $^{[6]}$Ti, green solid line). The zero energy corresponds to the lowest energy level of the unoccupied orbital including the core-hole effects and the experimental spectra are depicted for comparison. Light blue and red spheres represent Ti and O.

parent KTO crystal and KTO colloidal suspension formed through hydrothermal treatment. The former and latter spectra were measured in transmission and fluorescence modes, respectively. The spectrum of six-coordinated $^{[6]}TiO_2$ rutile is depicted in Fig. 4a for reference. The edge-jump for each spectrum was normalized to the average intensity after the subtraction of the background absorption. The three characteristic absorption peaks (or the pre-edge feature) at 4970–4975 eV are labeled A, A_1, A_2, etc. based on the literature.[31–34] In the Ti *K*-edge XANES spectra, the pre-edge feature at 4970–4975 eV is related to the Ti 1*s* to 3*d* transition, and its intensity is associated with the density of unoccupied Ti 3*d*-O 2*p* hybridized states. The 1*s* to 3*d* transition is basically forbidden by dipole selection rules but becomes allowed when *p*–*d* orbital mixing occurs in a site without a center of symmetry. That is, the 1*s* to 3*d* transition is strongly related to the coordination symmetry around the Ti atom given the dipole approximation, which is forbidden in octahedral symmetry; however, it is allowed in tetrahedral and square pyramidal symmetry as a result of 3*d*–4*p* orbital mixing, and the reader is referred to literature examples of theoretical and experimental results regarding this point.[31–34] In the XANES spectrum, the parent KTO shows a pre-edge peak at approximately 4970.5 eV (feature A, Fig. 4a), which corresponds to the Ti 1*s*–3*d* transition. After the hydrothermal treatment, three noticeable changes were observed in the spectrum of the KTO colloidal nanosheet suspension. First, the pre-edge peak was shifted to higher energies by approximately 0.4 eV. It is well recognized that the pre-edge peak position of Ti species is dependent on the CN of Ti species, in which the peak positions of $^{[5]}$Ti and $^{[6]}$Ti are approximately 4970.5 and 4970.9–4971.7 eV.[31,32] Secondly, weak shoulder peaks appeared at approximately 4974.3 and 4975.4 eV, and these resemble the A_2 feature of TiO_2 rutile. Third, the intensity of the pre-edge peak decreased by approximately 20% after the hydrothermal treatment. Similar spectral changes after immersion in nitric acid have been reported for $K_2{}^{[5]}TiO_3$ crystals because the coordination polyhedron around Ti^{4+} changes from square pyramidal to distorted octahedral as a result of the additional hydronium ions in the acidic solution.[6]

We next calculated the theoretical spectra of KTO and their derivatives, including the core-hole effects, and compared them with the experimental spectra. Herein, we introduce a model compound of a hydrated KTO derivative, $K_2{}^{[5,6]}Ti_2O_5$-H_2O, the crystal structure of which is shown in Fig. S7. $K_2Ti_2O_5$-H_2O is nominally formed through the following hydrolysis reaction: $K_2Ti_2O_5 + H_2O \rightarrow K_2Ti_2O_5$-$H_2O$, in which half of the five-coordinate Ti species in KTO become six-coordinate Ti in $K_2Ti_2O_5$-H_2O (Fig. S5, $^{[5]}$Ti:$^{[6]}$Ti = 1:1). Fig. 4b shows the calculated Ti *K*-edge XANES spectra of $K_2{}^{[5]}Ti_2O_5$ and $K_2{}^{[5,6]}Ti_2O_5$-H_2O, where the core-hole position for each model is shown in Fig. S1. The lattice parameters for $K_2{}^{[5]}Ti_2O_5$ obtained by geometry optimization were a = 1.1394951 nm, b = 0.378495 nm, and c = 0.651370 nm and β = 99.85314°, which agrees well with the experimental data, and these parameters were used for the XANES spectra simulation. The theoretical spectral features (peak number, intensity, and shape) for $K_2{}^{[5]}Ti_2O_5$ in the pre-edge region resemble those of the experimental spectrum (black solid lines in Fig. 4a and 4b). When the core-hole is formed on the six-coordinate $^{[6]}$Ti species in $K_2Ti_2O_5$-H_2O (Fig. S1b), the intensity of the pre-edge peak becomes low because of the dipole selection rule (1*s* to 3*d* transition), and the peak is divided into two peaks. On the other hand, as shown in Fig. S1c, putting the core-hole on the five-coordinate $^{[5]}$Ti forced one pre-edge peak to slightly shift to lower energy by 0.3 eV compared with that for $K_2{}^{[5]}Ti_2O_5$. Thus, the

Table 1 Exfoliation energies of $K_2Ti_2O_5$, $K_2Ti_2O_5$–H_2O, and $K_2Ti_4O_9$ based on DFT calculations.

Entry	Sample	$\Delta E_{exfoliation}$ (meV/Å^2)
1	$K_2Ti_2O_5$	21.7
2	$K_2Ti_2O_5$–H_2O	12.9
3	$K_2Ti_4O_9$	103.1

intensity of the pre-edge peak on $K_2Ti_2O_5$-H_2O decreased by around 40% and the position of the pre-edge peak was shifted by approximately 0.3 eV to lower energies (green solid line in Fig. 4b). The experimental spectrum of the KTO nanosheets (blue solid line in Fig. 4a) is not completely understood nor was it successfully simulated using the model compound $K_2Ti_2O_5$-H_2O, but, based on the three points mentioned above, the geometries of some of the Ti species in the nanosheet colloid are octahedral. We consider the following two possibilities: (i) $^{[6]}Ti^{4+}$ with octahedral geometry and $^{[5]}Ti^{4+}$ with pyramidal geometry coordinated with a hydroxyl group are both present in the KTO nanosheet or (ii) $^{[5]}Ti^{4+}$ having pyramidal geometry in the colloid is coordinated by hydronium ions to form a quasi-octahedral environment similar to that of the $K_2{}^{[5]}TiO_3$ crystal.[6] Again, note that KTO crystals undergo hydrolysis in water and water molecules are easily readily accommodated in the interlayers.

We then calculated the exfoliation energies, $\Delta E_{exfoliation}$, of $K_2Ti_2O_5$, $K_2Ti_2O_5$–H_2O, and $K_2Ti_4O_9$ following a literature method.[24,25] The slab models of each compound are shown in Fig. S2, and the results are summarized in Table 1. The $\Delta E_{exfoliation}$ values for $K_2Ti_2O_5$, $K_2Ti_2O_5$–H_2O, and $K_2Ti_4O_9$ were calculated to be 21.7, 12.9, and 103.1 meV/Å^2, respectively. Mounet et al. classified bulk 3D geometrically layered compounds into three groups: (i) "easily exfoliable", (ii) "potentially exfoliable", and (iii) "high binding energy".[25] $K_2Ti_2O_5$, $K_2Ti_2O_5$–H_2O, and $K_2Ti_4O_9$ belong to groups (ii), (i), and (iii), respectively. The value (12.9 meV/Å^2) obtained for $K_2Ti_2O_5$–H_2O is somewhat lower than those of MoS_2 (approximately 20 meV/Å^2) and BN (approximately 19 meV/Å^2),[25] which are easily exfoliable in common organic solvents.[7] Another interesting point is that the $\Delta E_{exfoliation}$ value for $K_2Ti_2O_5$ and $K_2Ti_2O_5$–H_2O is about one-fifth or less of that of $K_2Ti_4O_9$, which is consistent with the experimental results shown in Fig. 2.

Based on the experimental and theoretical analysis, we now discuss the exfoliation of KTO crystals without the use of acids and bases. A comparison of possible K–O bonds having lengths <3.10 Å in $K_2Ti_2O_5$, $K_2Ti_2O_5$–H_2O, and $K_2Ti_4O_9$ is shown in Fig. 5. In this visualization, one K^+ cation nominally interacts with four framework oxygen ions through electrostatic interactions, where K^+ is located in the approximately 5-Å diameter pockets built from six oxygen species in the interlayer galley space (Fig. 5a). Notably, three-fourths of the oxygen ions are located on the same side of the metalate framework, which could decrease the exfoliation energy. Further, the hydrolysis of $K_2Ti_2O_5$ changed the coordination mode of the K^+ cations in the interlayers. That is, one K^+ cation hardly

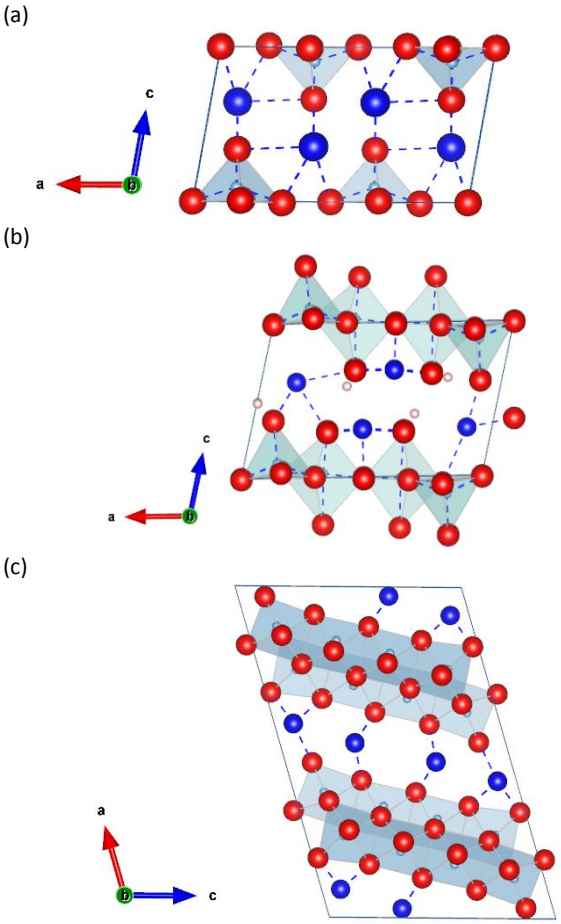

Fig. 5 Crystal structures and K-O bonds in layered titanate: (a) $K_2Ti_2O_5$, (b) $K_2Ti_2O_5$–H_2O, and (c) $K_2Ti_4O_9$. Dashed line, K–O bonds having bond lengths < 3.10 Å. Blue, light blue, red, and pink spheres represent K, Ti, O, and H, respectively.

interact with the oxygen ions located on the opposite side of the metalate framework within 3.10 Å. The lowest $\Delta E_{exfoliation}$ of $K_2Ti_2O_5$–H_2O among the three compounds can be attributed to this coordination change. On the other hand, K^+ in $K_2Ti_4O_9$ is tightly sandwiched between the metalate layers, leading to a higher exfoliation energy. The present findings indicate the importance of the coordination environment around interlayer ions for the efficient exfoliation of layered compounds. Interestingly, the formation of hydroxyl groups on the surface of host compounds can significantly reduce the exfoliation energy, and this could be an effective approach for exfoliation.

Conclusions

Single-crystalline KTO crystals of millimeter size were grown from a KCl–KOH mixed flux using a flux-evaporation assisted method. Thirteen types of solvents with different functional groups were examined for the exfoliation of the KTO crystals without the use of acids and bases, and H_2O was found to be the best dispersion medium. The use of hydrothermal treatment on KTO crystals at 120 °C for 3 days in water

resulted in exfoliation. The characterization results indicated that the lateral size of the KTO nanosheet was 5–15 μm, and the thickness for approximately 60% of nanosheets was less than 10 nm. The XANES results indicated a change in the local structures of some of the Ti species in the KTO through the hydrothermal treatment, wherein the CN of the Ti species was changed from five to six. The exfoliation energies for the KTO and hydrated KTO derivative were calculated to be 21.7 and 12.9 meV/Å^2, respectively, based on DFT calculations. These values are much lower than those for $K_2Ti_4O_9$ (103.1 meV/Å^2), agreeing well with the experimental results. Thus, the introduction of hydroxyl groups to the material surface could be an effective approach for the exfoliation of layered compounds.

Author Contributions

F.H. and K.T. conceived the idea and designed the research. F.H., K.F., N.T., T.S., and C.T. performed the crystal growth, exfoliation, and characterization experiments. F.H., M.K., H.S., H.T., and M.K. performed the DFT calculation. F.H. wrote the first draft of the paper, and all of the authors discussed and commented on the paper. All the authors have approved the final version of the manuscript.

Conflicts of interest

There are no conflicts to declare.

Acknowledgements

This work was supported by the Japan Society for the Promotion of Science (JSPS) KAKENHI (Nos. 20K05074 and 20H05214) and the Program for Building Regional Innovation Ecosystems of the Ministry of Education, Culture, Sports, Science, and Technology (MEXT), the Center of Innovation Program “Global Aqua Innovation Center for Increasing Water Sustainability and Improving Living Standards in the World” of the Japan Science and Technology Agency (JST) JST COI Grant Number JPMJCE1316, R1WD11, -12, -13, and the Environment Research and Technology Development Fund 5RF-1902 of Environmental Restoration. The XAFS experiments were performed at beamline BL5S1 of the Aichi Synchrotron Radiation Center, Aichi Science & Technology Foundation, Aichi (Proposal No. 2020D4025) and at beamline BL-12C of the Photon Factory, High Energy Accelerator Research Organization KEK under the approval of the Photon Factory Program Advisory Committee (Proposal No. 2018G632).

Notes and references

1 V. Nicolosi, M. Chhowalla, M. G. Kanatzidis, M. S. Strano and J. N. Coleman, *Science*, 2013, **340**, 1226419.
2 C. Tan, X. Cao, X. J. Wu, Q. He, J. Yang, X. Zhang, J. Chen, W. Zhao, S. Han, G. H. Nam, M. Sindoro and H. Zhang, *Chem. Rev.*, 2017, **117**, 6225.
3 C. N. R. Rao, H. S. S. Ramakrishna Matte and U. Maitra, *Angew. Chem., Int. Ed.*, 2013, **52**, 13162.
4 K. Noda, Y. Igarashi, H. Imai and Y. Oaki, *Chem. Commun.*, 2021, **57**, 5921.
5 L. Wang and T. Sasaki, *Chem. Rev.*, 2014, **114**, 9455.
6 Y. Masubuchi, R. Miyazaki, H. Kikuchi, T. Motohashi and S. Kikkawa, *Dalton Trans.*, 2014, **43**, 13751.
7 J. N. Coleman, M. Lotya, A. O'Neill, S. D. Bergin, P. J. King, U. Khan, K. Young, A. Gaucher, S. De, R. J. Smith, I. V. Shvets, S. K. Arora, G. Stanton, H.-Y. Kim, K. Lee, G. T. Kim, G. S. Duesberg, T. Hallam, J. J. Boland, J. J. Wang, J. F. Donegan, J. C. Grunlan, G. Moriarty, A. Shmeliov, R. J. Nicholls, J. M. Perkins, E. M. Grieveson, K. Theuwissen, D. W. McComb, P. D. Nellist and V. Nicolosi, *Science*, 2011, **331**, 568.
8 D. L. Druffel, K. L. Kuntz, A. H. Woomer, F. M. Alcorn, J. Hu, C. L. Donley and S. C. Warren, *J. Am. Chem. Soc.,* 2016, **138**, 16089.
9 M. Tournoux, R. Marchand and L. Brohan, *Prog. Solid State Chem.*, 1986, **17**, 33.
10 S. Andersson and A.D. Wadsley, *Nature*, 1960, **187**, 499.
11 T. Sasaki, M. Watanabe, H. Hashizume, H. Yamada and H. Nakazawa, *J. Am. Chem. Soc.*, 1996, **118**, 8329.
12 N. Miyamoto,K. Kuroda and M. Ogawa, *J. Mater. Chem.*, 2004, **14**, 165.
13 M. Zukalová, M. Kalbáč, L. Kavan, I. Exnar and M. Graetzel, *Chem. Mater.*, 2005, **17**, 1248.
14 Y. Fujiki and T. Ohsaka, *J. Ceram. Assoc. Japan*, 1982, **90**, 27.
15 B. Ravel and M. Newville, *J. Synchrotron Radiat.*, 2005, **12**, 537.
16 S. J. Clark, M. D. Segall, C. J. Pickard, P. J. Hasnip, M. I. J. Probert, K. Refson and M.C. Payne, *Zeitschrift fur Krist.*, 2005, **220**, 567.
17 T. Ishimoto Y. Ito, T. Tada, R. Oike, T. Nakamura, K. Amezawa and M. Koyama, *Solid State Ionics*, 2016, **285**, 195
18 T. Mizoguchi, I. Tanaka, S. P. Gao and C. J. Pickard, *J. Phys. Condens. Matter*, 2009, **21**, 104204.
19 G. Kresse and J. Furthmüller, *Phys. Rev. B-Condens. Matter Mater. Phys.*, 1996, 54, 11169.
20 G. Kresse and J. Furthmüller, *Comput. Mater. Sci.,* 1996, **6**, 15.
21 J. P. Perdew, K. Burke and M. Ernzerhof, *Phys. Rev. Lett.*, 1996, **77**, 3865.
22 J. P. Perdew, A. Ruzsinszky, G. I. Csonka, O. A. Vydrov, G. E. Scuseria, L. A. Constantin, X. Zhou and K. Burke, *Phys. Rev. Lett.*, 2008, **100**, 136406. *Phys. Rev. Lett.* 2009, **102**, 039902.
23 P.E. Blöchl, *Phys. Rev. B*, 1994, **50**, 17953.
24 B. N. N. Silva, S.R. Tavares and A.A. Leitão, *New J. Chem.*, 2020, **44**, 10111.
25 N. N. Mounet, M. Gibertini, P. Schwaller, D. Campi, A. Merkys, A. Marrazzo, T. Sohier, I. E. Castelli, A. CepellottiG. Pizzi and N. Marzari, *Nat. Nanotechnol.*, 2018, **13**, 246.
26 K. Momma and F. Izumi, *J. Appl. Crystallogr.*, 2011, **44**, 1272
27 C. E. Bamberger, G.M. Begun and C.S. MacDougall, *Appl. Spectrosc.*, 1990, **44**, 30.
28 Q. Wang and J. S. Chung, *Appl. Catal. A Gen.*, 2009, **358**, 59
29 G. B. Saupe, C. C. Waraksa, H. N. Kim, Y. J. Han, D. M. Kaschak, D. M. Skinner and T.E. Mallouk, *Chem. Mater.*, 2000, **12**, 1556
30 M. Lotya, A. Rakovich,J. F. Donegan and J. N. Coleman, *Nanotechnology*, 2013, **24**, 265703.
31 F. Farges, G. E. Brown and J. J. Rehr, *Geochim. Cosmochim. Acta*, 1996, **60**, 3023.
32 F. Farges and G. E. Brown, *Phys. Rev. B-Condens. Matter Mater. Phys.*, 1997, **56** , 1809.
33 D. Cabaret, A. Bordage, A. Juhin, M. Arfaoui and E. Gaudry, *Phys. Chem. Chem. Phys.*, 2010, **12**, 561.
34 N. Jiang, D. Su and J. C. H. Spence, *Phys. Rev. B-Condens. Matter Mater. Phys.*, 2007, **76**, 214117.